Intensifying the synthesis of starch nanoparticles using ultrasound-assisted acid hydrolysis method

Vikas S Hakke
National Institute of Technology
Shirish Sonawane (shirish@nitw.ac.in)
National Institute of Technology Warangal https://orcid.org/0000-0002-3201-6731
Sivakumar Manickam
Universiti Teknologi Brunei
Sami Boufi
University of Sfax
Dipak V Pinjari
University of Mumbai
G Uday Bhaskar Babu
National Institute of Technology
Shriram S Sonawane
Visvesvaraya National Institute of Technology Nagpur

Research Article

Keywords: Acid hydrolysis, Starch, Nanoparticles, Ultrasound, Crystallinity

Posted Date: February 19th, 2021

DOI: https://doi.org/10.21203/rs.3.rs-212091/v1

Abstract

In the present study, an intensified approach for the synthesis of starch nanoparticles (SNPs) was demonstrated by using ultrasound-assisted acid hydrolysis method. The conventional acid hydrolysis for the synthesis of SNPs was intensified using ultrasound. The overall time required to convert starch granules to SNPs in the conventional acid hydrolysis method (48 h) was significantly reduced to 45 min by simultaneous acid hydrolysis and ultrasound irradiation. The acid concentration was found to be an important parameter for obtaining the desired size and morphology of the synthesized SNPs. The variation in the surface charges associated with the SNPs was confirmed through measuring their zeta potential. These potential charges on the surface of SNPs induce crystal growth among the synthesized nanoparticles. The irregular crystal morphology at higher acid concentration clearly shows SNPs' attachment with each other by coalescence. The higher crystallinity for SNPs was observed at low acid concentration; however, the lower acid concentration (0.5 M) leads to the smaller particle size of SNPs from 40 to 60 nm, with the overall yield of 23%. The proposed ultrasound method is more efficient and reproducible for the synthesis of SNPs for various applications.

Introduction

Starch is a polysaccharide, abundantly found in plants, and can be utilized as biopolymers in various applications, such as an additive in the food processing industry. The synthesis of starch nanoparticles (SNPs) and their effective utilization for the various applications such as carrier for curcumin delivery [1], antioxidants [2], drugs and many more had been studied interestingly during the last decade. The insoluble, semi-crystalline nature of native starch consists of two homopolymers, namely amylose and amylopectin. These homopolymers of glucose construct the structure of native starch, which is highly complex. Thus, the functionality of starch particles shows variations even though they come from the same source [3,4] . Concerning the structural complexity, amylose is essentially linear, whereas amylopectin is a highly branched structure linked to a minimum of 20-25 straight-chain residues [5]. These structural variations of amylose and amylopectin in the starch particles induce variations in their shape, size, and crystallinity. Among the most common types of starch, the weight percentage of amylose ranges from 42% to 82%. In contrast, the amylopectin ranges from 18 to 28%, and depending on its plant source, starch raw materials have different chemical composition [6]. The starch granule’s morphology and size were found to be based on the amylopectin's branch length and distribution [4].

The nanosized particles of a material display unique properties such as a higher surface area to volume ratio than their macro-sized particles. Several methods, such as enzymatic treatment [7], acid hydrolysis [8], mini emulsion [9], and mechanical degradation [10] are reported to synthesize nanosized starch particles starting from its native form. The conventional acid hydrolysis is more efficient as it generates a smaller starch particle size [11–13]. In the acid hydrolysis of starch, SNPs synthesis is affected by the size of native starch particles and acid interaction time. A remarkable enhancement by 50% in starch particle’s crystallinity was found after 10 days of acid hydrolysis [14]. It was observed that the initial size of particles could promote the hydrolysis. The resultant SNPs from the hydrolysis process were found to

possess enhanced crystallinity, making SNPs thermally stable compared to native starch particles. This leads to the usefulness of SNPs in the food processing industry. The isolated starch filtrates from the suspension of acid consists of nanoscale starch with higher crystallinity than native starch. The process is easier but consumes more time for the conversion of starch granules in to the nanoscale. In this context, there is a need for an alternative approach to reduce the time required for the synthesis of SNPs.

The smaller sized starch particles offered lower resistance to proton transfer in the inner layers and enhanced the extent of hydrolysis [15]. The hydrolysis rate was found to differ from 60 to 90% depending upon the type of starch. Also, the short chains of amylose and amylopectin were generated during the hydrolysis of starch [16]. But the limitation associated with acid hydrolysis is that it is a time-consuming process, and more importantly, the yield is below 15%. Precipitation in the microemulsion system was successfully utilized to control SNP's particle size in the prefixed environment [17]. It has been observed that the spherical shape of SNPs is predominant as compared to other shapes with uniform size distribution within 80-90 nm. The nanoprecipitation method was also adapted to synthesize SNPs in size range of 110-140 nm [18]. The role of the surfactant and oil phase is more critical concerning nanoemulsion and microemulsion systems. The rate of mechanical agitation also altered the size distribution of SNPs in both the above processes. Vahanian et al. [19] observed that enzymatic pretreatment through diffusion reduces the time for the synthesis of SNPs via conventional acid hydrolysis method. They found a significant reduction of time from 5 days to 45 h for the preparation of SNPs. They also noted that the yield is 15% within 20 h. Cross-flow filtration was also an efficient way to separate SNPs from the bulk suspension [20]. The above method assisted in improving the quality of SNPs by separation. SNPs yield and homogeneity was found to enhance without modifying the crystalline structure of SNPs and aggregation. This process is also economical and energy-efficient than the conventional method. The extrusion was another method by which SNPs were synthesized, and increased efficiency was achieved using appropriate crosslinkers. The synthesized SNPs were more stable with a crosslinker, even at around 100 ^{o}C [21].

Ultrasound irradiation induces the scission of native starch particles by reducing the length of amylose and amylopectin branches. The mechanical impact of cavitation proceeded with a lower yield; one reason could be the starch molecule's different chain pattern. The different configurations of amylose and amylopectin reduced the process yield [22]. The mechanical reduction of the native starch particle was an effective method to obtain its nanosize [2,11]. A.R. Jambrak et .al [23] observed that temperature control was essential to avoid gel formation during ultrasonic irradiation. The SNPs exhibited characteristic gel formation at higher temperatures by associating with water to form a film [24].

Ultrasound-assisted acid hydrolysis, a hybrid method, was reported in several studies. It is a fast and efficient way of synthesizing SNPs without compromising starch particle's crystallinity [2,25]. Sami et al. [26] , it has been noted that the formed SNPs could be modified by surface treatment, which was utilized as a carrier for various applications. Jambrak et al. [23] reported the negative effect of ultrasound irradiation on food material, where, the generated free radicals due to ultrasound influences the food material negatively. Subjecting starch particles to acoustic cavitation leads to the destruction of granular

structure, due to which the amorphous phase of the particle immediately contacts the acid solution. The mechanical effect of cavitation produced by sound waves proceeds with the generation and collapse of saturated and unsaturated cavities in solution. These cavities collapse and generate high pressures and temperatures locally, which is responsible for breaking a longer chain of the starch structure. It was also found that the input energy requirement is less due to cavitation effects [23]. However, the starch particle's water absorption capacity was enhanced as the time of ultrasound irradiation increased. This is due to the destruction of the starch particle from cavitation effects, allowing water to penetrate and retain in the starch particles. After subjecting to ultrasound irradiation, two layers of starch suspension were noted; one was in the nanoscale while the other was in the microscale [27]. These microscale starch particles were found to be smaller than that of native starch particles. Nearly 12% of particles were SNPs, and the remaining 88% were microscale particles. The synthesized SNPs had lower thermal stability as compared to micro-scale starch particles. SNPs synthesized by ultrasound approach was found to be effective as compared to the conventional acid hydrolysis process [11]. This process's main advantage is that, the SNPs in the range from 20 to 80 nm were obtained without any chemical modification on cost of high energy requirement for the synthesis. However, the ensuing SNPs were amorphous, and acid concentration as well as employing high-intensity sonication for more than 1 h were necessary to ensure a good SNPs yield. This process did not require any additional steps after washing. SNPs were achieved using high intensity ultrasound and concentrated acid concentration, and a yield of 21% was reported with acid concentration of about 4.5 M [28]. SNPs were also achieved by the esterification of waxy corn starch through 120 min of ultrasonic irradiation [29]. The ultrasound method was found to affect the crystalline structure of SNPs, which demonstrated potential applications in food, biotech, and materials industries. High-intensity ultrasound irradiation of starch suspension converted starch particles in the micron to the nano scale in less than 100 min at 25 ^{o}C [28].

Although the synthesis of SNPs using the conventional acid hydrolysis method has the merits of displaying better crystallinity of SNPs; however, reduction in size, lower yield, and more extended time of processing are the critical issues. Hence, an effective alternative method has to focus on improving the process by boosting the yield and reducing reaction time. The enzymatic or mini-emulsion, and extrusion processes exhibit some of the advantages, but the isolation of SNPs from the downstream solution becomes challenging. Following this, ultrasound-assisted acid hydrolysis shows improvements in the yield (23%) and reduces the processing time (45 min). The process intensification by strategic transformation of the conventional acid hydrolysis of starch to synthesize SNPs has been achieved and is a more efficient and green process. In this intensified process, acid concentration optimization is essential, as the hydrolysis of starch granules plays a vital role in synthesizing SNPs. In the present work, for SNPs synthesis, different acid concentrations were used to hydrolyze starch particles under ultrasonic irradiation for overall enhancement in SNPs yield, reduction in size, and processing time. The acid concentration was varied from 0.5 to 3 M. Overall, this study's framework offers an intensified approach for synthesizing SNPs for various commercial applications such as food additives, nanofillers for packaging materials, etc.

Materials And Methods

2.1 Materials

The native cornstarch (amylose content 65-73%, granular size 5-17 μm) and sulphuric acid (93-98% pure) were purchased from Alfa Aesar (Thermo Fisher Scientific Ltd., India). All chemicals were used as supplied.

2.2 Synthesis of starch nanoparticles (SNPs)

Initially, the acid solutions (sulphuric acid, 50 mL) of different concentrations (0.5 M, 1 M, 2 M, and 3 M) were prepared using deionized water. First, starch powder (1.5 g) was dispersed uniformly in the acid solution using ultrasonic irradiation for 45 min. For this process, a probe sonicator (20 kHz, probe tip diameter 2 cm, 220 W, pulse mode 3 sec on and 1 sec off, Dakshin ultrasonicator, Mumbai, India) was employed. The temperature of the system was maintained at 15 ^{o}C, by immersing in a thermostatic bath. Starch irreversibly changes its structure at a temperature above 60 ^{o}C and thus to avoid gelatinization the solution was mainly kept at a lower temperature [30]. The temperature of the bath was controlled by the continuous supply of cold water at 10 ^{o}C. The solution was neutralized after sonication with NaOH (0.25 M) as at pH 7 termination of hydrolysis is achieved. The starch solution was then centrifuged in two-stages. At first, centrifugation at 800 rpm for 2 min was done to separate microscale starch particles from the suspension. The obtained microscale starch particles were then dried, and the weight of particles was noted to calculate the process yield. Then, the supernatant of the first stage was centrifuged again at 9000 rpm for 15 min. The precipitate obtained from this second stage was then washed by deionized water to obtain the acid-free SNPs. Further, the precipitate slurry was dried in the desiccator to obtain dry SNPs.

For comparison, the synthesis of SNPs was also carried out by the conventional method of acid hydrolysis. For this, acid hydrolysis of native starch was carried out using 3 M sulphuric acid and agitation (300 rpm) through magnetic stirring for 48 h. After 2 days of acid hydrolysis, the obtained SNP suspension was neutralized and centrifuged. The precipitated SNPs were then dried using a desiccator, and the yield of SNPs was calculated on a dry weight basis. The acid hydrolysis of starch is slower due to which we compared the 45 min hybrid acid hydrolysis method with a 48 h conventional acid hydrolysis method to understand the effect of ultrasound.

2.3 Characterization of SNPs

2.3.1 Particle size analysis and Zeta potential measurements

The particle size distribution (PSD) and Zeta potential analysis of SNPs were carried out at room temperature (25 °C). Dynamic light scattering (DLS) was used for the measurement of PSD of suspensions. For this, the required amount of SNPs was dispersed in water to obtain a dispersion of starch. The Malvern Zeta sizer Nano (ZS, ZEN 3600) was used to measure PSD and zeta potential. The

zeta potential of synthesized SNPs was measured at constant pH value of 9. The stability of SNPs in the suspension was assessed using the suspended SNPs zeta potential in solution.

2.3.2 Morphology of SNPs

The SNP's morphological characteristics were revealed using transmission electron microscopy (TEM) and scanning electron microscopy (SEM). TEM imaging (TEM instrument, PHILIPS, CM 200) was run at 200 kV and a resolution of 2.4 A°. The TEM micrographs of the fabricated SNPs were utilized to study their surface morphology. The sample for TEM analysis was prepared by spreading a drop of the SNPs suspension (0.2% w/v) on a glow discharged carbon coated grid. To conduct SNP's SEM analysis, SEM (TESCAN-Vega 3 LMU model microscope, Fuveau, France) operating at an accelerating voltage of 20 kV was used. The particle size of synthesized SNPs at different concentration of acid, was confirmed by SEM and TEM image analysis of SNPs. The minimal count of 450 was consider while calculating the mean diameter of SNP.

2.3.3 X-ray diffraction (XRD) analysis of SNPs

The preconditioning of native starch and SNPs were achieved in a desiccator at a relative humidity of 35% for 3 days. The preconditioning is necessary to maintain the moisture content in the sample before XRD analysis. The Bruker D8 advanced diffractometer using copper Kα (Cu Kα) radiation (λ = 0.154 nm) was used. The intensity was recorded in the range of 4^{o}-50^{o} (2θ) with a step size of 0.018 and measuring for 2 sec. per point. The XRD spectra were also utilized to estimate and quantify the relative crystallinity of the synthesized SNPs. The crystallinity index of SNPs was calculated, as indicated earlier [31]. The sample's crystallinity was quantitatively estimated according to the method reported by Nara and Komiya [32]. A curve connecting the baselines of the peaks is drawn on the diffraction pattern. It is assumed that the area above the curve corresponds to the crystal domain, and the lower area corresponds to the amorphous part. The ratio of the upper area to the total area indicates the crystallinity

2.3.4 Fourier Transform Infrared Spectroscopy (FTIR) of SNPs

The FTIR spectra (Shimadzu-8400 FTIR instrument, Japan) were obtained using the KBr pellet method. KBr was mixed with SNPs, and the mixture was converted into a pellet for the analysis. The spectral resolution was 4/cm, whereas the scanning range was 4000-400 cm^{-1} to record the FTIR spectrum.

2.3.5 Determination of thermal degradation properties of SNPs

Thermal degradation of SNPs was carried out with TGA-6/DTG of NETZSCH STA 2500 (precision of temperature measurement ±2 °C, microbalance sensitivity <5 µg). The percentage weight loss of the SNPs was recorded continuously as a function of temperature, under dynamic conditions, in the range of 30-600 °C. The experiments were carried out at atmospheric pressure, under a nitrogen atmosphere, with a flow rate of 50 mL/min, at a linear heating rate of 10 °C/min. The small mass of the sample, i.e., 15 mg

was filled in the crucible, whereas the reference crucible was kept empty in case of native starch and SNPs. The experiment was carried out in triplicate to check the reproducibility of results.

2.3.6 Water absorption capacity of SNPs

The water absorption and binding capacity of SNPs were calculated based on the dry weight of SNPs. SNPs known weight (S_1) was dispersed into deionized water (5% solution, 25 mL) using magnetic stirring for 30 min at 30 ^{o}C. After 30 min, the solution was cooled, and the separation of SNPs was carried out after 24 h by nanofiltration. The separated SNPs were filtered and dried at room temperature in a desiccator. The weight of the obtained SNPs was noted (S_2). The weight of water absorbed in the starch nanoparticles was calculated using the following Eq. 1.

$$Absorpition\ of\ water\ in\ SNPs\ (\%) = \frac{(S_2 - S_1)}{S_2} * 100 \qquad (1)$$

Results And Discussion

3.1 Particle size distribution and stability of SNPs in suspension

The obtained SNPs using the ultrasound-assisted hydrolysis method were evaluated for particle size distribution (PSD), and stability using the dynamic light scattering (DLS) measurements. The comparative particle size distribution is shown in Figure 1. The conventional acid hydrolysis was performed for 48 h using a high acid concentration of 3 M. The ultrasound-assisted hydrolysis process was more efficient than the conventional hydrolysis [2,24,25]. The size of native starch particles was reduced when subjected to sonication. The native starch conversion only with ultrasound was attempted by Bel Haaj et al. [11]. The native starch was reduced in the range of 30 nm to 100 nm with the application of continuous high power ultrasound irradiation for 75 min. In this study, acid hydrolysis notably assists ultrasound irradiation for the rapid hydrolysis with minimum irradiation time was observed.

The particle size was observed in the range of 500-600 nm in the conventional method, after 48 h of hydrolysis. In contrast, in the case of ultrasound treated starch hydrolysis, the particle sizes were below 200 nm, and notably, it was applied only for 45 min. A reduction in the synthesis time of SNPs arises from the sonication effects. The cavities generated in the starch suspension during sonication collapse with high impact, producing higher local temperatures and pressures. These cavities collapse randomly in the solution. When they collapse near or on the starch particle's surface, the high impact physically damages starch surfaces, increasing acid diffusion inside the starch particles. The hydrolysis rate is found to increase due to higher acid diffusion in the starch particles, reducing the hydrolysis time in the synthesis of SNPs. The suspended starch particles in the solution gain the energy from the impacts and due to which agglomeration rate amongst starch granules hindered with great amount. The only

drawback with sonication is the rise in local temperature during the collapse of cavities, inducing starch gelatinization [30]. Thus, extensive temperature control is necessary to avoid the gelatinization effect in the starch particles. The reported study, noted that the gelatinization of native starch occurs in temperature range of 60 to 80 ^{o}C [33].

Figure 1 shows the effect of acid concentration on the SNPs size distribution. As the acid concentration increases, the particle size of SNPs also increases. This increase in particle size, with an increase in acid concentration, is due to SNPs simultaneous agglomeration during hydrolysis [25]. The collapse of cavities in the solution increases the temperature and pressure suddenly for a fraction of time. This collapse induces the dissociation of water and acid in the form of free radicals. A rapid rise in temperature and pressure due to the collapse of cavities generates high energy, which is higher than the bond dissociation energy of water and sulphuric acid, leading to the generation of free hydroxyl ($\cdot$OH) radicals from water and sulphonic group (-SO_2-OH) [34]. These radicals are reactive, and their presence on the surface of SNPs was confirmed from infrared spectrometry and increased zeta potential. These charged sulphonic groups are responsible for the repulsive force between SNPs when they are lower in number. The esterification of the surface hydroxyl groups of SNPs with sulfuric acid is another side reaction that continues to the generation of sulfate groups on SNPs, as reported in the preparation of starch nanocrystals [35]. As the concentration of sulphuric acid increases, the sulphonic group's radicals also increases, leading to the simultaneous crystal growth of the starch in the suspension. The higher the charge more will be the nanoparticles interaction in the suspension, higher the rate of agglomeration. From Figure 2**,** it could be observed that as the acid concentration decreases, the suspension becomes clear and transparent. At the lower acid concentration, SNPs were more stable in the suspension, scattered and lower rate of agglomeration is clearly observed. However, as the concentration of acid increases the haziness of solution slightly increases, this is possibly due to SNP interactions as soon as they produced in the solution. Due to the agglomeration of SNP at higher concentration suspension becomes hazy. The acid interaction with starch particles plays an important role during its simultaneous exposure to sonication. The cavities generated during sonication create a high impact that breaks the structure of starch, allowing the penetration of acid into the inner cores of starch. The amorphous portion of starch reacts with acid and breaks its branches, reducing the complexity of starch structure [15,16]. Hence, the reduction in the size of starch particles is due to both acid interaction and sonication. The ultrasound application causes acid interaction more effectively with the amorphous part of the starch. Simultaneously, it also generates free radicals in the suspension which interact with the surface of starch, as confirmed from the peaks of the functional groups of FTIR [27,36]. The starch molecule with a minimum of three hydroxyl groups at the outer side and the associated two branched amylopectins react with $H_2SO_{4,}$ and a family of hydroxyethers and hydroxyethanal was synthesized from amylopectin. The branched structure of amylopectin offers a weaker bond for the acid reaction. The reaction further proceeds by reacting with amylose.

SNPs were found to be more stable in the ultrasound-assisted hydrolysis process as compared to the conventional method. The minimal SNPs size was in the range of 50-70 nm with the average particle size

(PSD) of 63 nm. **Table 1** shows the variations in the stability of each SNPs in the suspension. The sonication assists in the physical destruction of starch particles and reduces the agglomeration rate of SNPs. As the physical destruction of granules does not directly involving in chemical conversion of amylose, thus ultrasound does not have significant effect on the crystallinity of SNPs [11]. The yield of the synthesized SNPs demonstrates a decreasing trend as the acid concentration increases. The yield (based on dry mass) includes the losses during the process. The maximum yield of 23% was obtained using an acid concentration of 0.5 M, which is optimized in terms of acid concentration as well as ultrasound irradiation time as compared to the earlier report [11,28], where an acid concentration of 3.16 M was employed. However, the conventional acid hydrolysis shows the yield between 10 and 20%, depending on the hydrolysis time and origin of starch, with the same acid concentration and hydrolysis time. TEM was used to understand the morphology of the lowest SNPs, whereas all the remaining samples were observed under SEM.

Acid interaction with starch particles can be divided into three stages. In the first mild stage, acid interacts with the outer surface of starch particles. In the second intermediate stage, where the starch's outer surface slightly distracts, and diffusion of acid to the inner part of the starch could be observed. This diffusion enhances the hydrolysis rate as the amorphous phase of starch is exposed to acid. The amorphous amylose linear chain breaks down faster than that of the crystalline branched structure of amylopectin. In the third stage of hydrolysis, acid interacts with the amylopectin of starch. The destruction of amylopectin induces the gelatinization effect in the starch suspension. Thus, acid interaction with starch particles plays a vital role in the production of SNPs.

The time of acid interaction with starch particles may impact the particle size of the synthesized SNPs. Subjecting the suspension to high-frequency ultrasound irradiation for 45 min generates OH^- radicals and $^-OH\text{-}SO_2$ functional groups interact with the SNPs surface. These radicals and charged ions contribute to the potential for the dispersed SNPs in solution. The synthesized SNPs exhibited good stability in the water suspension as observed from their zeta potential values at pH 9, which is similar to the already reported observations [13,17]. More water molecules dissociate to give hydroxyl radicals at lower acid concentration, due to which the potential of SNPs with lower acid concentration was observed in the range of -21 to +21 mV, at constant pH value of 9, indicating a more stable structure in the suspension, and were observed to reduce as the concentration of acid increases. Zeta potential of SNPs indicates the negative charge on the surface, making them valuable carrier of anions in medical applications. The colloidal phase of all the synthesized SNPs exhibits a narrow size distribution as the suspension's polydispersity index is below 0.7. A suspension of colloidal nanoparticles below a polydispersity index of 0.7 with narrow size distribution and better colloidal stability has been reported [37].

3.2 Morphologies of the SNPs

The closely packed structure of starch is classified in three types- A, B, and C [38]. TEM and SEM micrographs are shown in Figure 3, which reveal the SNP’s morphologies synthesized using different acid concentrations and ultrasonic irradiation. The Type A crystals shows closely packed structure, with lower

volume, whereas B types of crystalline structure are loosely packed. The mixed A & B types of crystalline nature shown by the C-type crystal structures. Figure 3a shows the differentiation of two different types of crystalline structures of SNPs. Imberty and Perez [38] reported that a closely packed A-type starch nanocrystal shows higher resistance for the impingement of acid than that of B-type starch nanocrystal. Figure 3a shows the two different types of SNPs synthesized during hydrolysis. It was very clear that, the mixed crystalline structures of SNPs were synthesized. The random impact of cavities collapse and intensity of acid interaction at the surface are the prominent reasons for the randomness of the particle size. The average particle size determined by the DLS method was supported by the figure 3. The nanosized SNPs could be noted through TEM (Figure 3b). Figure 3 confirms that the synthesized SNPs are roughly spherical, elliptical in shape and uniform size distribution was not observed in the conventional acid hydrolysis method. The conventional acid hydrolysis produced mixed crystallinity which is C-type crystallinity. A similar morphology of SNPs has already been reported [11,26]. The spherical particles of SNPs with the short-chain arrangement are visible in TEM (Figure 3b) and are in the range of 40-60 nm. This is the smallest range of SNPs found at a lower concentration of acid (0.5 M). The A-type crystal was confirmed from TEM (figure 3b) and the x-ray diffraction pattern in figure 5a. The closely packed structure shows higher resistance to the further reduction of particle size with acid interaction. However, the SNPs at higher acid concentration are in the range of 100 to 250 nm, which were found to increase with the acid concentration. These SNPs were also observed under SEM (Figure 3 c, d, e, f). The aggregate in the solution shows a larger size of SNPs. The larger size aggregates of SNPs were found at an acid concentration of 3 M. SNP's morphological studies with SEM and TEM confirm the irregular size distribution associated with this synthesis process. SNP's size with 1 M acid concentration varies from the lowest (below 100 nm) to a maximum (above 200 nm). The randomness in the shape of the starch nanoparticles is due to the impact of cavities during ultrasound propagation and acid interaction. Figure 3 displays the oval, and spherical shape of SNPs, similar to the earlier reports [2,26,28].

The image analysis of the TEM and SEM images of synthesized SNP were carried out with minimum count of 370. The results of image analysis were noted in table 1. Though the hydrolysis rate is higher at the high acid concentration, the aggregation rate due to surface charges were found to be higher. The aggregates show higher resistance to the hydrolysis due to cumulative higher amylose content. This higher amylose content hinders the propagation of acid reaction. The image analysis shows almost similar results as generated from DLS based particle size analyzer. The crystalline types were significantly varying with the acid concentration. The acid interaction with starch granules was meaningfully guided by random collapses of cavities at the surface or near the surface of the starch granule. However, the size distribution was observed narrower, with slight exception with 2 M acid concentration. The image analysis of figure 3 [TEM and SEM] also confirms the same. The SNP size distribution was assessed by TEM, and SEM image analysis and reproduced in figure 4.

Variation in acid concentration significantly differ the SNP crystal morphology. The sonication effect provides the randomness in acid interaction with the starch granule due which to both A, B-type crystalline structure was produced. The frequency variation of ultrasound irradiation may be the additional parameter to study which can be considered for future studies. The high impact of cavity

collapse generates the random damage to the starch granule due to which loosely bounded B-type starch nanoparticle crystals population was observed in higher extent at all acid concentration.

3.3 X-ray diffraction (XRD) analysis of SNPs

The synthesized SNPs with different acid concentrations possess different crystalline structures. The effect of acid concentration on the crystallinity of SNPs was studied by using XRD diffraction. Figure 5 shows the comparison of the XRD spectrum for the SNPs synthesized using different concentrations of acid. A semi-crystalline nature of SNPs could be noted from this spectrum. The crystallinity of synthesized SNPs was affected by the acid concentration. The XRD spectrum shows a relatively high crystallinity of SNPs with the usage of ultrasound during acid hydrolysis as similarly reported earlier [11,25,26]. Ultrasound cavitation leads to the physical damage of native starch particles due to the high impact of cavities. This cavitation effect induces a rise in the rate of hydrolysis. The reduction in the amorphous phase of the native starch particles increases the crystallinity in the synthesized SNPs. The characteristic A-type diffraction patterns are seen at 15.220^{o}, 17.046^{o}, 17.973^{o}, 19.874^{o}, and 26.400^{o}. These significant peaks show variations with a change in acid concentration. The critical A-type and V-type spectra of SNPs are unaffected by varying the acid concentration. The crystallinity of SNPs was higher with the lowest concentration of acid, which could be due to the dominant effect of sonication. Figure 5 (d) shows the crystallinity effect on SNPs by the conventional acid hydrolysis. It is found that as the hydrolysis time increases, the crystallinity of starch granule also increases. The hydrolysis time for the conventional method is 48 h, whereas, for the ultrasound-assisted acid hydrolysis, it is only 45 min.

The crystallinity index (C_I) of the individual SNPs was calculated, as described earlier [31]. The crystallinity index between 17^{o} and 18^{o} for the SNPs was calculated and recorded as 0.57, 0.50, 048, 0.43, and 0.41 with an increase in the acid concentration. As reported, the crystallinity is a quantitative indicator of the crystallinity of particles. It has been found that the crystallinity of SNPs decreases as the acid concentration increases. The acid hydrolysis of starch can be divided into two major stages. The first one is a faster reaction of an acid with amylose, amorphous starch, and the other with the crystalline amylopectin. The acid reacts with linear molecules of amylose and converts this long chain of amylose to shorter forms. This reaction is faster due to the linear structure of amylose. However, amylopectin is a highly branched molecule with a short-chain. The second stage of hydrolysis progresses through an acid with crystalline amylopectin, which is slower than the first stage. At a lower acid concentration, some shorter chains of amylopectin distract by the cavitation effect.

Still, the hydrolysis of amorphous amylose is faster due to which the resultant crystallinity of SNPs is higher. Higher numbers of radicals are produced at higher acid concentration during sonication, which increases the hydrolysis rate in the first and second stages. The combined effect of sonication and free radicals for branched amylopectin hydrolysis affects the destruction of the branched structure, reducing the crystallinity of resultant SNPs. As the acid concentration increases the combined effect and hence the resultant crystallinity of SNPs also reduces. The relative crystallinity of SNPs reduces by 20 % as the acid concentration varies from 0.5 M to 1 M. Whereas, with a change in the acid concentration from 1 M to 2

M the relative crystallinity reduces only by 18 %. SNPs' crystallinity is more than native starch by 40%, as reported earlier [39,40]. The crystallinity of the SNPs synthesized at lower concentration was 42% more than that of native starch, which is higher than the previously reported value [23,41]. However, compared to native starches, the crystallinity of the SNPs increased because of reduction of amorphous part in starch due to acid interaction.

Although, in the X-ray diffraction comparison of synthesized SNPs, found that synthesized SNPs were of A-type crystals with only difference in the variation in the ratio amylose to amylopectin associated with the crystals. The cluster formed during agglomeration of SNPs cumulatively shows higher ratio of amylose to amylopectin. Whereas, at lower acid concentration rate of agglomeration is low.

3.4 Fourier Transform Infrared Spectroscopy (FTIR) of SNPs

As shown in Figure 6, FTIR was recorded to understand the percentage of light transmitted by the SNPs. This transmittance is used to identify the associated functional groups. The significant peak at 1650 cm^{-1} is due to the vibrational bond energy of the hydroxyl group. This peak associated with all SNPs confirms that the hydroxyl functional group is associated with SNPs. The S=O bond vibrations are seen at 1196 cm^{-1}, a characteristic peak confirming the presence of sulphonic group associated with SNPs [7]. The sulphonic functional group is not significantly found at a lower acid concentration. The presence of these functional groups also supports the results obtained from zeta potential measurements. The peak at 1097 cm^{-1} endorses the stretching of C-O-C bond associated with the structure of SNPs. The significant presence of sulphonic functional group associated with SNPs at higher acid concentration is responsible for the higher potential charges on the SNPs, which induce the agglomeration of nanoparticles, and hence the size of SNPs slightly increases.

3.5 Thermal degradation study of SNPs

The dehydration process during dry heating can be well understood by thermogravimetric analysis (TGA) of SNPs. Figure 7 presents the decomposition of SNPs, which probably can be divided into four stages of temperature. It was found that the thermographs of SNPs follow the same path almost, indicating that all the starch comes from the same botanical source. The only difference was the amount of energy required to achieve in every stage. The mass loss variation of SNPs may look different, as it is due to the variation in the structural orientation, which is due to different amounts of amylopectin and amylose associated with them. Thus, the crystallinity and the amorphous region in SNPs are different. This indicates that the SNPs granule, at higher concentrations, demonstrate a larger size due to coalescence, which required higher energy to separate water molecules from them. The SNP's pyrolysis in an inert atmosphere consists of the following steps as seen from the TGA, which was similar to as reported earlier [12]. The first stage with the mass loss is associated with unbound water evaporation. The amount of water molecules depends on the adsorption capacity of SNPs. The second stage of mass loss is associated with the loss of bonded water molecules, which could have been due to the hydroxyl groups of starch crystal leaving behind the ether group. Their presence was confirmed with the FTIR analysis, as indicated

in Figure 6**.** Larger the crystal size more are the number of hydroxyl groups, higher is the bounded water molecules synthesized, which require high energy for the second stage of mass loss. The thermal decomposition of organic compound was observed in the third stage of mass loss, followed by the fourth stage where it finally becomes ash. The TGA of SNPs clearly shows that SNPs at higher concentration has a higher amount of ether groups associated with them; thus, the second mass loss required higher enough than lower acid concentration. The crystalline structure at lower acid concentration has a lower tendency to agglomerate and has a lower amount of ether group associated with them. Thus, second mass loss was achieved slightly earlier than the other. This confirms the formation of smaller size SNPs at a low concentration of H_2SO_4 [42].

3.6 Water absorption capacity of SNPs

Water absorption was evaluated to examine the structural difference and molecular arrangements in the synthesized SNPs. High power ultrasound facilitates the acid hydrolysis of starch and isolates the hydrolyzed starch particles, besides avoiding agglomeration [2]. Also, the collision impact of ultrasound assists the mechanical breaking of the chain. The destruction of the complex molecular structure eases acid to enter the inner layers of starch which reacts with the amorphous phase of starch particles. The water absorption of SNPs is reported in Table 2**.** The decreasing water absorption capacity of SNPs could be noted as the acid concentration increases. At lower acid concentration, destruction of the particle due to ultrasound increases because of the high impact of cavities. This destruction, along with the hydrolysis of the starch's amorphous phase, generates voids in SNP's crystal. Smaller the size of starch particles higher is the percentage size of voids in the crystal. The water molecules diffuse through the outer layer of SNPs to inner layers and occupy these voids inside the crystal.

There is a weight difference of SNPs after water interaction for 24 h, because of the difference in the molecular arrangement and differences in the crystalline structure. As shown in Figure 8, the water absorption of SNP decreases as the SNP particle size increases. The water absorption depends upon the organization of the interior SNP crystals. The crystalline arrangement of starch depends on the amount of amylose and amylopectin. The water absorption shows a difference in the amylose and amylopectin contents of native starch and SNPs. This difference is due to acid interaction with starch particles [23,28]. The SNPs obtained through the conventional method have shown good absorption property, due to acid interaction time for 48 h, which significantly reduces the amorphous phase of the starch particles.

Conclusion

The present study demonstrates an intensified approach for the synthesis of SNPs using the ultrasound-assisted acid hydrolysis. The overall time of the process was reduced from 48 h to 45 min. A significant enhancement in the hydrolysis rate of starch particles due to cavitation effects has been noted. The smaller particle size and narrower particle distribution was noted as acid concentration reduces from 3 M to 0.5 M. The highest yield of 23% was noted at 0.5 M H_2SO_4 within 45 min of sonication time. The effects of acid concentration on the synthesized SNPs were examined and found to reduce the

synthesized SNP's crystallinity as the acid concentration increases. As compared to the native starch, the synthesized SNPs with a lower concentration of acid shows 43% higher crystallinity. The relative crystallinity reduces by 10% as the acid concentration increases from 0.5 M to 1 M. However, it reduces to 18% and 23% when acid concentration changes to 2 M and 3 M, respectively. The conventional acid hydrolysis has the highest interaction of acid with starch particles, even though SNP's relative crystallinity using conventional methods shows 20% lower relative crystallinity than the SNPs synthesized at a lower concentration. At the lowest acid concentration, SNPs in the size range of 40-60 nm were noted. Also, the size of SNPs slightly increased as the acid concentration increased. The critical peaks of the XRD spectrum confirm the synthesis of SNPs. The decreasing pattern of the crystallinity index of SNPs between 17^{o} and 18^{o}, as shown in the XRD spectrum, confirms that SNP's crystallinity decreases as the acid concentration increases. The variation in the thermal decomposition energy of SNPs, confirms SNPs of smaller size at lower acid concentration. The water absorption of SNPs demonstrates its affinity towards water. The presence of voids inside the SNPs could be responsible for water absorption. The present investigation provides a useful pathway for SNP's commercial production for various applications, for example, using them as nanofiller in the epoxy coating, encapsulation, and bio-sensitive packaging applications.

Declarations

Funding:

The authors are thankful to the International Bilateral Cooperation Division of Department of Science and Technology India, Ministry of Science and Technology India, for the financial support to execute the project at the National Institute of Technology Warangal, through India Tunisia Bilateral project grant no DST/INT/TUNISIA/P-06/2017.

Conflict of Interest:

The authors declare that they have no known competing financial interests or personal relationships that could have appeared to influence the work reported in this paper.

Authors' contributions: -

- Vikas Hakke synthesized the nanoparticles and conducted the analysis, collected most of the literature work under the direction of the corresponding authors and wrote the first draft of the manuscript
- Shirish Sonawane is the corresponding authors and contributed to improving the quality of the manuscript by reviewing and providing intellectual input.
- Sivakumar Manickam and Sami Boufi are the authors and contributed to improving the quality of the manuscript by reviewing and providing intellectual input.

- Dipak V Pinjari, G Uday Bhaskar Babu, and, Shriram Sonawane provided intellectual inputs to improve the quality of the final submitted manuscript.

References

[1] L.S. Rajeswari, S.N. Moorthy, K.N. Rajasekhran, Preparation of Cassava Starch Nanoparticles and their Application as a Carrier System for Curcumin Delivery, Int. J. Nanotechnol. Appl. 5 (2011) 193–201. http://www.ripublication.com/ijna.htm.

[2] S. Shabana, R. Prasansha, I. Kalinina, I. Potoroko, U. Bagale, S.H. Shirish, Ultrasound assisted acid hydrolyzed structure modification and loading of antioxidants on potato starch nanoparticles, Ultrason. Sonochem. 51 (2019) 444–450. doi:10.1016/j.ultsonch.2018.07.023.

[3] A. Buléon, P. Colonna, V. Planchot, S. Ball, Starch granules: Structure and biosynthesis, Int. J. Biol. Macromol. 23 (1998) 85–112. doi:10.1016/S0141-8130(98)00040-3.

[4] N. Masina, Y.E. Choonara, P. Kumar, L.C. du Toit, M. Govender, S. Indermun, V. Pillay, A review of the chemical modification techniques of starch, Carbohydr. Polym. 157 (2017) 1226–1236. doi:10.1016/j.carbpol.2016.09.094.

[5] A. Dufresne, Crystalline starch based nanoparticles, Curr. Opin. Colloid Interface Sci. 19 (2014) 397–408. doi:10.1016/j.cocis.2014.06.001.

[6] F. Zhu, Composition, structure, physicochemical properties, and modifications of cassava starch, Carbohydr. Polym. 122 (2015) 456–480. doi:10.1016/j.carbpol.2014.10.063.

[7] H. Zhang, Y. Tian, Y. Bai, X. Xu, Z. Jin, Structure and properties of maize starch processed with a combination of α-amylase and pullulanase, Int. J. Biol. Macromol. 52 (2013) 38–44. doi:10.1016/j.ijbiomac.2012.09.030.

[8] D. Le Corre, J. Bras, A. Dufresne, Starch nanoparticles: A review, Biomacromolecules. 11 (2010) 1139–1153. doi:10.1021/bm901428y.

[9] M.A. El-Sheikh, New technique in starch nanoparticles synthesis, Carbohydr. Polym. 176 (2017) 214–219. doi:10.1016/j.carbpol.2017.08.033.

[10] S. Elazzouzi-hafraoui, Y. Nishiyama, J.L. Putaux, L. Heux, F.F. Dubreuil, C. Rochas, The shape and size distribution of crystalline nanoparticles prepared by acid hydrolysis of native cellulose, Biomacromolecules. 9 (2008) 57–65. doi:10.1021/bm700769p.

[11] S. Bel Haaj, A. Magnin, C. Petrier, S. Boufi, Starch nanoparticles formation via high power ultrasonication, Carbohydr. Polym. 92 (2013) 1625–1632. doi:10.1016/j.carbpol.2012.11.022.

[12] Y.J. Wang, V. Den Truong, L. Wang, Structures and rheological properties of corn starch as affected by acid hydrolysis, Carbohydr. Polym. 52 (2003) 327–333. doi:10.1016/S0144-8617(02)00323-5.

[13] S. Wang, L. Copeland, Effect of Acid Hydrolysis on Starch Structure and Functionality : A Review, Crit. Rev. Food Sci. Nutr. 55 (2015) 1081–1097. doi:10.1080/10408398.2012.684551.

[14] S. Kumari, B.S. Yadav, R.B. Yadav, Synthesis and modification approaches for starch nanoparticles for their emerging food industrial applications: A review, Food Res. Int. 128 (2020) 108765. doi:10.1016/j.foodres.2019.108765.

[15] B.B. Sanchez de la Concha, E. Agama-Acevedo, M.C. Nunez-Santiago, L.A. Bello-Perez, H.S. Garcia, J. Alvarez-ramirez, Acid hydrolysis of waxy starches with different granule size for nanocrystal production, J. Cereal Sci. 79 (2018) 193–200. doi:10.1016/j.jcs.2017.10.018.

[16] H.Y. Kim, J.H. Lee, J.Y. Kim, W.J. Lim, S.T. Lim, Characterization of nanoparticles prepared by acid hydrolysis of various starches, Starch/Staerke. 64 (2012) 367–373. doi:10.1002/star.201100105.

[17] H.Y. Kim, S.S. Park, S.T. Lim, Preparation, characterization and utilization of starch nanoparticles, Colloids Surfaces B Biointerfaces. 126 (2015) 607–620. doi:10.1016/j.colsurfb.2014.11.011.

[18] S.F. Chin, S.C. Pang, S.H. Tay, Size controlled synthesis of starch nanoparticles by a simple nanoprecipitation method, Carbohydr. Polym. 86 (2011) 1817–1819. doi:10.1016/j.carbpol.2011.07.012.

[19] E. Vahanian, A. Dufresne, J. Bras, Enzymatic Pretreatment for Preparing Starch Nanocrystals, Biomacromolecules. 13 (2012) 132–137. doi:10.1021/bm201333k.

[20] D. Lecorre, J. Bras, A. Dufresne, Ceramic membrane filtration for isolating starch nanocrystals, Carbohydr. Polym. 86 (2011) 1565–1572. doi:10.1016/j.carbpol.2011.06.064.

[21] D. Song, Y.S. Thio, Y. Deng, Starch nanoparticle formation via reactive extrusion and related mechanism study, Carbohydr. Polym. 85 (2011) 208–214. doi:10.1016/j.carbpol.2011.02.016.

[22] R. Czechowska-biskup, B. Rokita, S. Lotfy, Degradation of chitosan and starch by 360-kHz ultrasound, Carbohydr. Polym. 60 (2005) 175–184. doi:10.1016/j.carbpol.2004.12.001.

[23] A.R. Jambrak, Z. Herceg, D. Subaric, J. Babic, M. Brncic, S.R. Brncic, T. Bosiljkov, D. Cvek, B. Tripalo, J. Gelo, Ultrasound effect on physical properties of corn starch, Carbohydr. Polym. 79 (2010) 91–100. doi:10.1016/j.carbpol.2009.07.051.

[24] S. Boufi, S.B. Haaj, A. Magnin, S.B. Haaj, A. Magnin, F. Pignon, G. Mortha, Ultrasonic assisted production of starch nanoparticles : Structural characterization and mechanism of disintegration, Ultrason. - Sonochemistry. (2017). doi:10.1016/j.ultsonch.2017.09.033.

[25] V.S. Hakke, U.D. Bagale, S. Boufi, G.U.B. Babu, S.H. Sonawane, Ultrasound Assisted Synthesis of Starch Nanocrystals and It's Applications with Polyurethane for Packaging Film, J. Renew. Mater. 08 (2020) 239–250. doi:10.32604/jrm.2020.08449.

[26] S. Boufi, S. Bel Haaj, A. Magnin, F. Pignon, M. Impéror-Clerc, G. Mortha, Ultrasonic assisted production of starch nanoparticles: Structural characterization and mechanism of disintegration, Ultrason. Sonochem. 41 (2018) 327–336. doi:10.1016/j.ultsonch.2017.09.033.

[27] A.F.K. Minakawa, P.C.S. Faria-Tischer, S. Mali, Simple ultrasound method to obtain starch micro- and nanoparticles from cassava, corn and yam starches, Food Chem. 283 (2019) 11–18. doi:10.1016/j.foodchem.2019.01.015.

[28] A. Mohammad Amini, S.M.A. Razavi, A fast and efficient approach to prepare starch nanocrystals from normal corn starch, Food Hydrocoll. 57 (2016) 132–138. doi:10.1016/j.foodhyd.2016.01.022.

[29] A. Garcia-gurrola, S. Rincon, A.A. Escobar-puentes, A. Zepeda, J.F. Pérez-robles, F. Martinez-bustos, Synthesis and succinylation of starch nanoparticles by means of a single step using sonochemical energy, Ultrason. - Sonochemistry. (2019). doi:10.1016/j.ultsonch.2019.04.035.

[30] Y. Liu, J. Yu, L. Copeland, S. Wang, S. Wang, Gelatinization behavior of starch: Reflecting beyond the endotherm measured by differential scanning calorimetry, Food Chem. 284 (2019) 53–59. doi:10.1016/j.foodchem.2019.01.095.

[31] S.H.D. Hulleman, M.G. Kalisvaart, F.H.P. Janssen, H. Feil, J.F.G. Vliegenthart, Origins of B-type crystallinity in glycerol-plasticized, compression-moulded potato starches, Carbohydr. Polym. 39 (1999) 351–360. doi:10.1016/S0144-8617(99)00024-7.

[32] S. Nara, T. Komiya, Studies on the Relationship Between Water-satured State and Crystallinity by the Diffraction Method for Moistened Potato Starch, Starch - Stärke. 35 (1983) 407–410. doi:10.1002/star.19830351202.

[33] Y. Qin, C. Liu, S. Jiang, L. Xiong, Q. Sun, Characterization of starch nanoparticles prepared by nanoprecipitation: Influence of amylose content and starch type, Ind. Crops Prod. 87 (2016) 182–190. doi:10.1016/j.indcrop.2016.04.038.

[34] S. Boufi, H. Kaddami, A. Dufresne, Mechanical performance and transparency of nanocellulose reinforced polymer nanocomposites, Macromol. Mater. Eng. 299 (2014) 560–568. doi:10.1002/mame.201300232.

[35] J.L. Putaux, S. Molina-Boisseau, T. Momaur, A. Dufresne, Platelet nanocrystals resulting from the disruption of waxy maize starch granules by acid hydrolysis, Biomacromolecules. 4 (2003) 1198–1202. doi:10.1021/bm0340422.

[36] Y. Jin, N. Hengl, S. Baup, F. Pignon, N. Gondrexon, M. Sztucki, A. Romdhane, A. Guillet, M. Aurousseau, Ultrasonic assisted cross-flow ultrafiltration of starch and cellulose nanocrystals suspensions: Characterization at multi-scales, Carbohydr. Polym. 124 (2015) 66–76. doi:10.1016/j.carbpol.2015.01.073.

[37] C.M. Patel, M. Chakraborty, Z.V.P. Murthy, Fast and scalable preparation of starch nanoparticles by stirred media milling, Adv. Powder Technol. 27 (2016) 1287–1294. doi:10.1016/j.apt.2016.04.021.

[38] A. Imberty, S. Perez, A revisit to the three-dimensional structure of B-type starch, Biopolymers. 27 (1988) 1205–1221. doi:https://doi.org/10.1002/bip.360270803.

[39] H.Y. Kim, J.A. Han, D.K. Kweon, J.D. Park, S.T. Lim, Effect of ultrasonic treatments on nanoparticle preparation of acid-hydrolyzed waxy maize starch, Carbohydr. Polym. 93 (2013) 582–588. doi:10.1016/j.carbpol.2012.12.050.

[40] D. Le Corre, H. Angellier-Coussy, Preparation and application of starch nanoparticles for nanocomposites: A review, React. Funct. Polym. 85 (2014) 97–120. doi:10.1016/j.reactfunctpolym.2014.09.020.

[41] D. LeCorre, J. Bras, A. Dufresne, Influence of botanic origin and amylose content on the morphology of starch nanocrystals, J. Nanoparticle Res. 13 (2011) 7193–7208. doi:10.1007/s11051-011-0634-2.

[42] N. Lin, J. Huang, A. Dufresne, Preparation, properties and applications of polysaccharide nanocrystals in advanced functional nanomaterials: A review, Nanoscale. 4 (2012) 3274–3294. doi:10.1039/c2nr30260h.

Tables

Table 1 The stability studies using average particle size and zeta potential measurement of SNPs through DLS

SNPs	H_2SO_4 concentration (M)	Average size (nm)	Average zeta potential (mV)	Yield (%)	Time of hydrolysis (min)	Mean size of the Particle with Image analysis nm	Total number of counts
SNP ultrasound-assisted hydrolysis 0.5M	0.5	63	-21.6	23	45	78	379
SNP ultrasound-assisted hydrolysis 1 M	1	102.6	-19.8	19	45	117	489
SNP ultrasound-assisted hydrolysis 2 M	2	207.1	-12.5	17	45	203	523
SNP ultrasound-assisted hydrolysis 3 M	3	323.4	-8.5	17	45	339	576
SNP conventional hydrolysis	3	629.3	0	17	48 h	623	692

Table 2 The water absorption capacity of SNPs

SNPs with the concentration of H_2SO_4	Time of ultrasonication (min)	Water Absorption (%)
0.5 M	45	13
1 M	45	11
2 M	45	10
3 M	45	8
3 M (conventional method - 48 h)	0	9

Figures

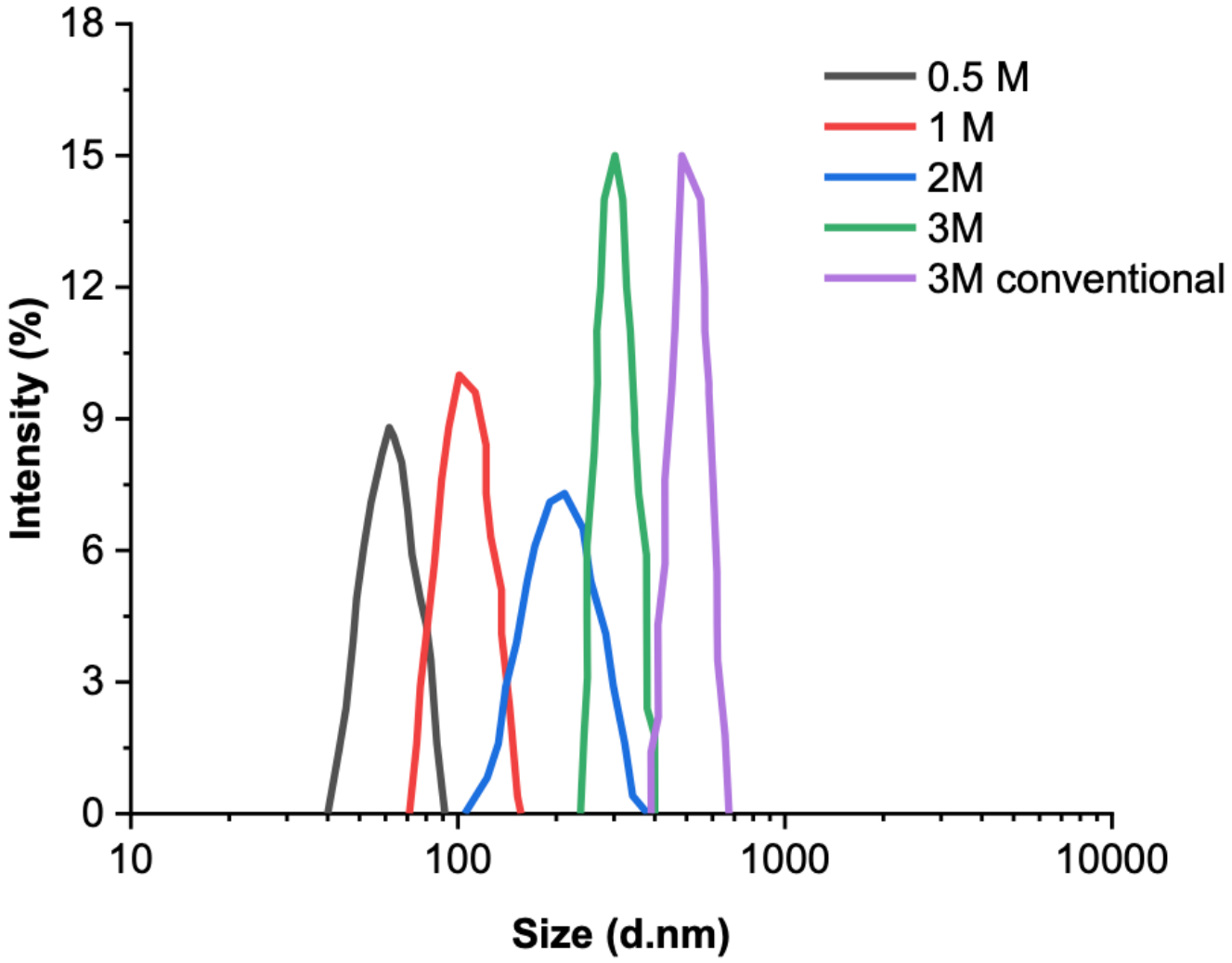

Figure 1

The particle size distribution of starch nanoparticles

Figure 2

The suspension of SNPs after hydrolysis for 45 min and before neutralization with NaOH solution

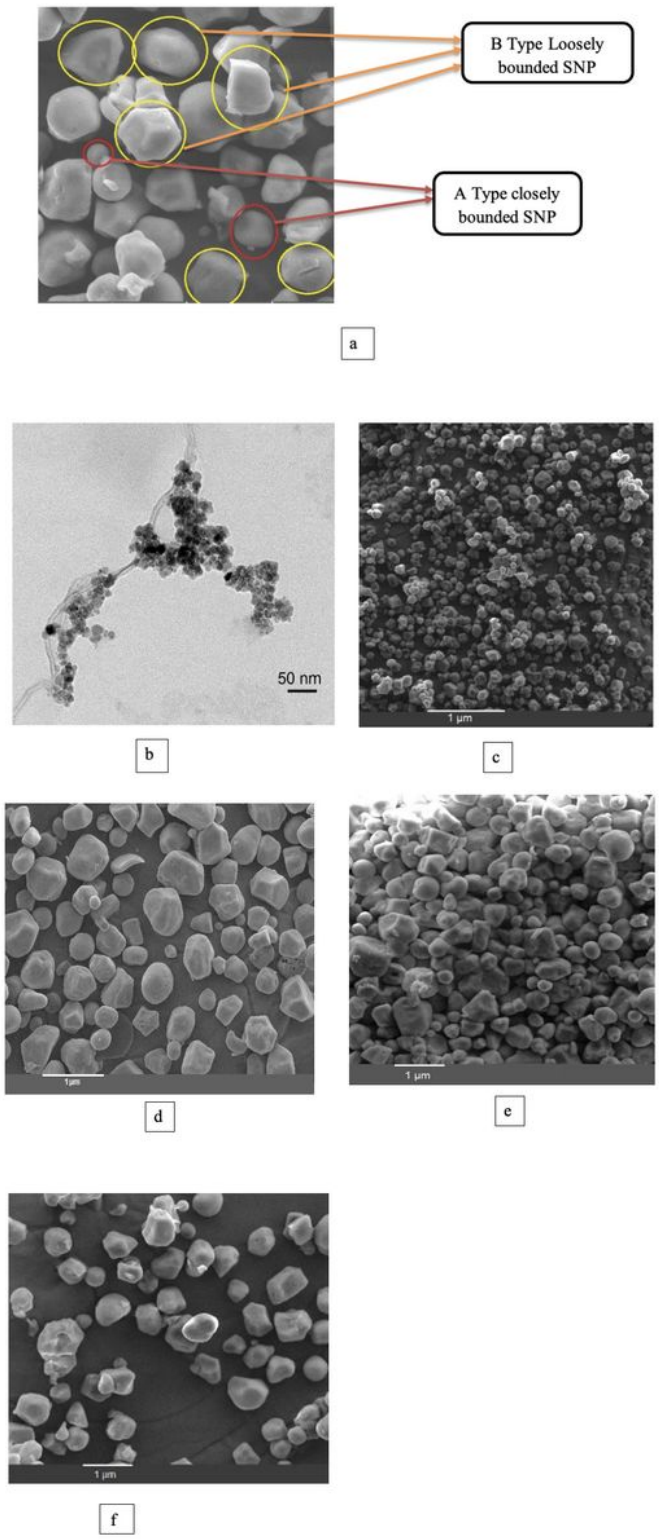

Figure 3

(a) The Different types of crystalline morphology synthesized during acid hydrolysis (b) TEM of SNPs with 0.5 M H2SO4 (c) SEM of SNPs with 1 M H2SO4 (d) SEM of SNPs with 2 M H2SO4 (e) SEM of SNPs with 3 M H2SO4 (f) SEM of SNPs with 3 M H2SO4 by the conventional method

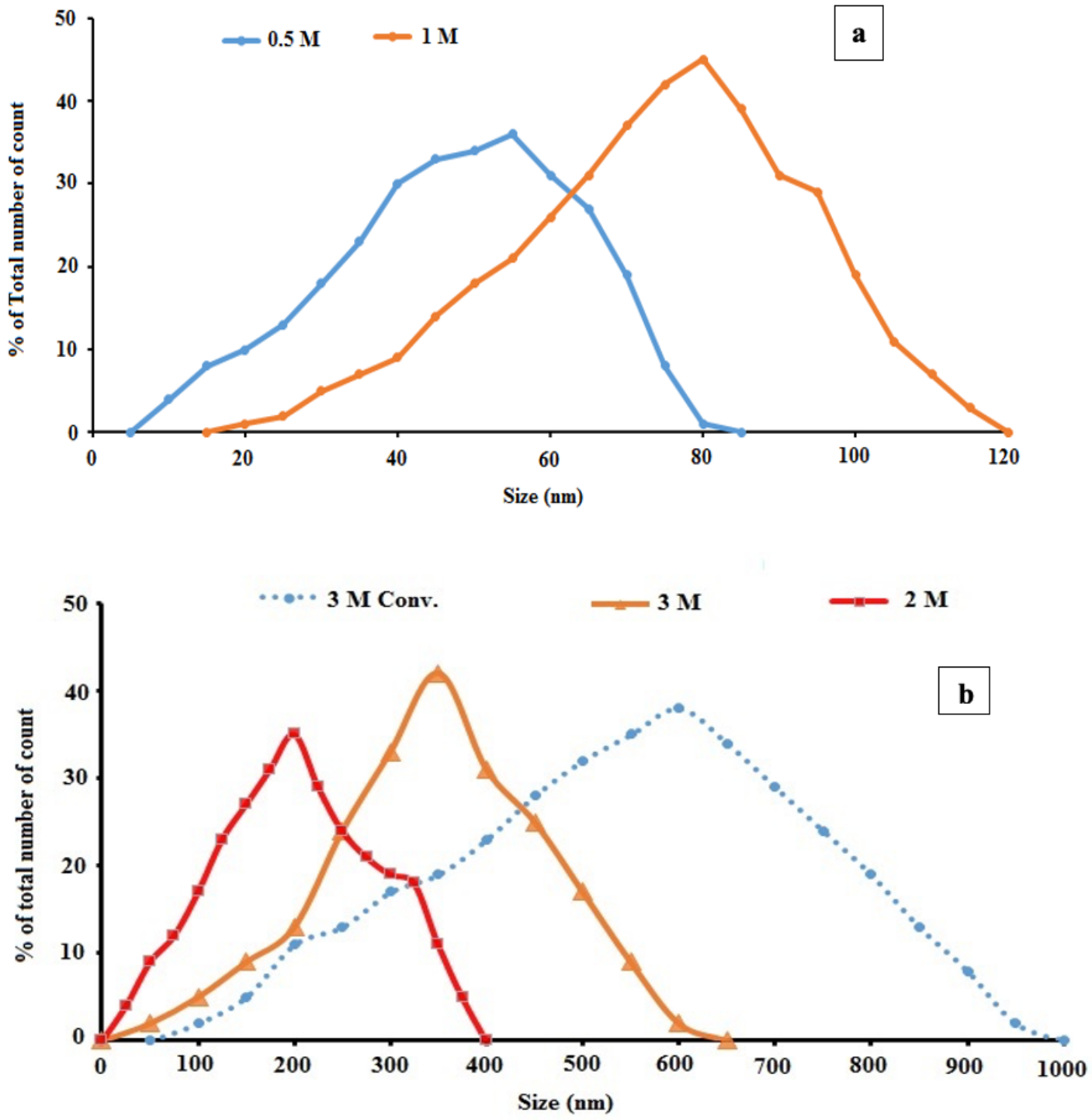

Figure 4

particle size distribution predicted by image analysis (a) for 0.5 M & 1 M concentration synthesized SNPs, (b) for 2 M, 3 M and 3 M conventional method synthesized SNPs. (b) XRD spectra of SNPs synthesized using 0.5 M and 2 M H2SO4

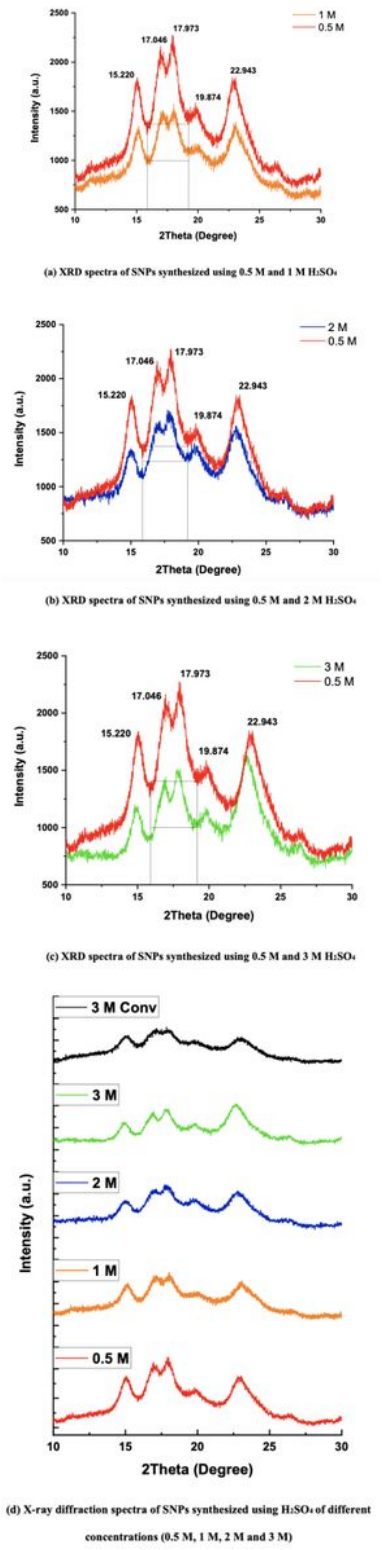

Figure 5

X-ray diffraction spectra of SNPs synthesized using different concentration of acid (a) XRD spectra of SNPs synthesized using 0.5 M and 1 M H2SO4. (b) XRD spectra of SNPs synthesized using 0.5 M and 2 M H2SO4 (c) XRD spectra of SNPs synthesized using 0.5 M and 3 M H2SO4. (d) X-ray diffraction spectra of SNPs synthesized using H2SO4 of different concentrations (0.5 M, 1 M, 2 M and 3 M).

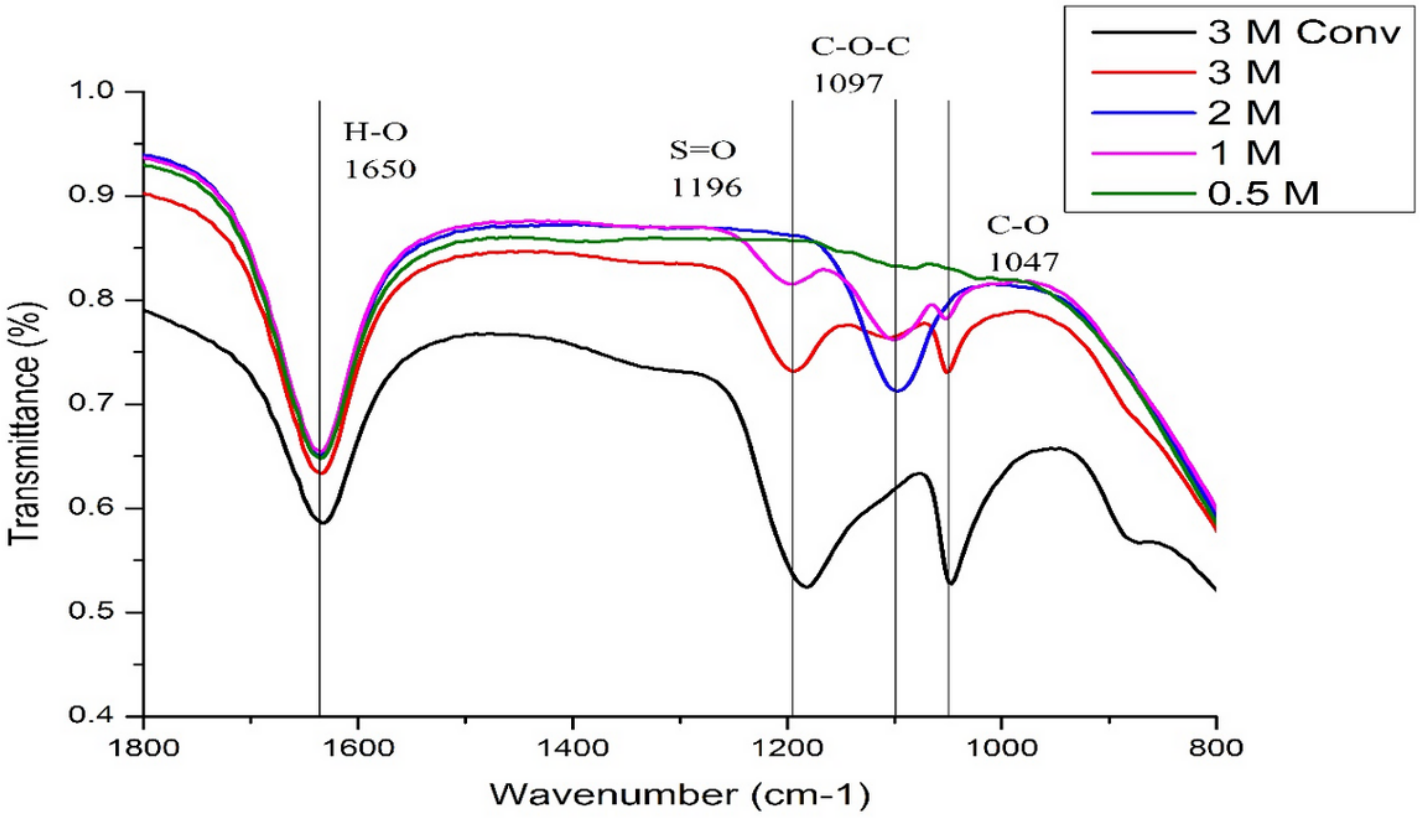

Figure 6

Fourier Transform Infrared spectra (FT-IR) of SNP synthesized using H2SO4 of different concentrations

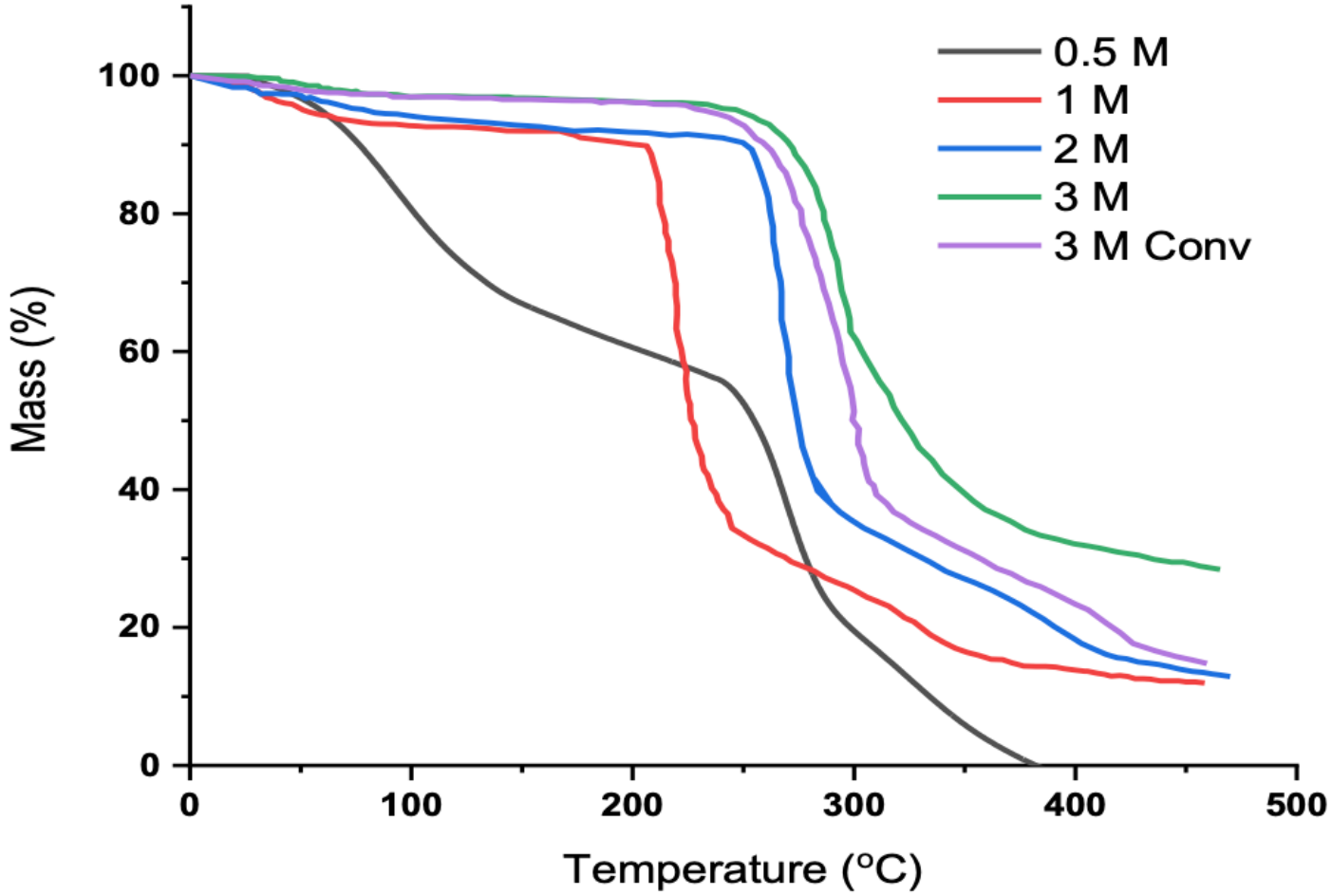

Figure 7

Thermal degradation studies of the synthesized SNPs.

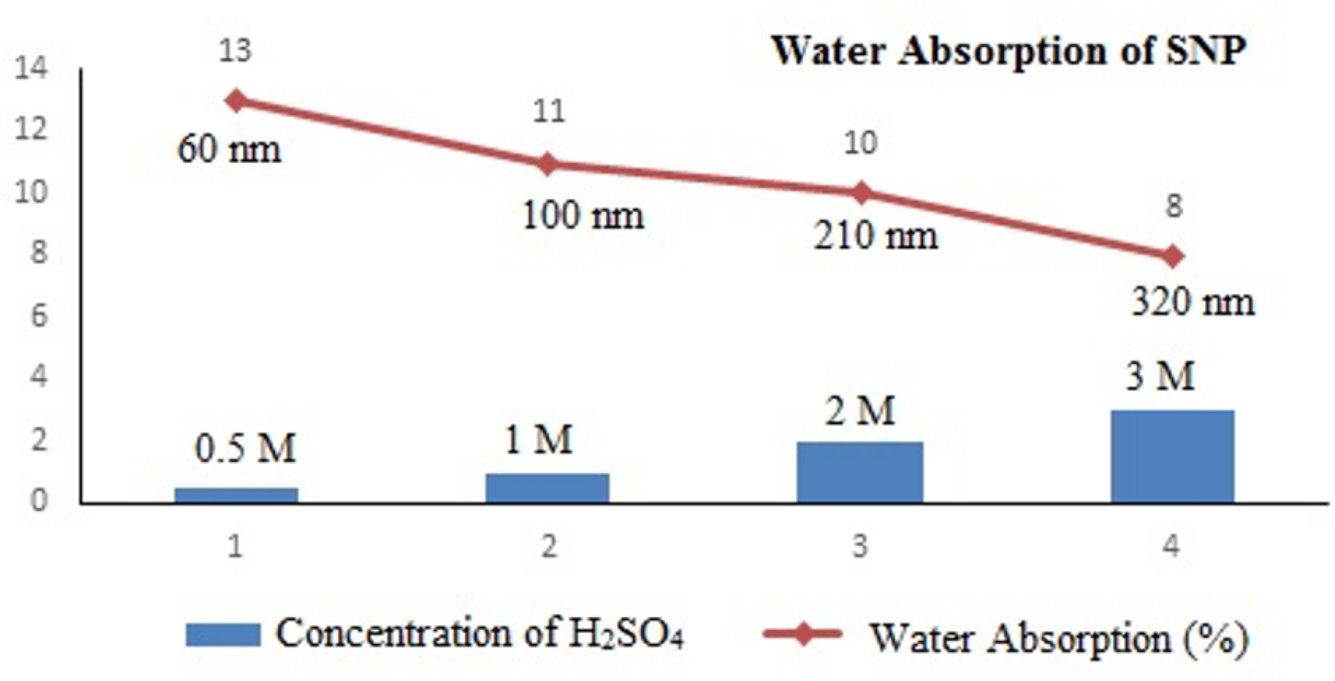

Figure 8

Water Absorption of SNPs synthesized using acid of different concentrations